Article

Not peer-reviewed version

Mitigating Diabetes and Gut Dysmotility in Mice: Long-Term Safety and Efficacy of miR-10a/B Treatment with No Indication for Cancer and Inflammation Risks

Rajan Singh , Se Eun Ha , Hahn Sung Park , Sushmita Debnath , Hayeong Cho , Gain Baek , Tae Yang Yu , Seungil Ro *

Posted Date: 3 January 2024

doi: 10.20944/preprints202401.0255.v1

Keywords: miR-10a-5p, miR-10b-5p, diabetes, gastrointestinal dysmotility, cancer, inflammation

Article

Mitigating Diabetes and Gut Dysmotility in Mice: Long-Term Safety and Efficacy of miR-10a/b Treatment with no Indication for Cancer and Inflammation Risks

Rajan Singh [1,†], Se Eun Ha [1,†], Hahn Sung Park [1], Sushmita Debnath [1], Hayeong Cho [1], Gain Baek [1], Tae Yang Yu [1] and Seungil Ro [1,2,*]

[1] Department of Physiology and Cell Biology, School of Medicine, University of Nevada, Reno, NV, 89557, USA

[2] RosVivo Therapeutics, Applied Research Facility, 1664 N. Virginia St., Reno, NV 89557, USA

* Correspondence: Seungil Ro, PhD, Professor, Department of Physiology and Cell Biology, University of Nevada School of Medicine, Center of Molecular Medicine Building L-207E, 1664 North Virginia Street, MS 575, Reno, NV 89557, Tel: 775-784-1462, Fax: 775-784-6903, Email: sro@med.unr.edu

† Rajan Singh and Se Eun Ha contributed equally to this work.

Abstract: Background/Aim: microRNAs (miRNAs) are key regulators of both physiological and pathophysiological mechanisms in diabetes and gastrointestinal (GI) dysmotility. Our previous studies have demonstrated the therapeutic potential of miR-10a-5p mimic and miR-10b-5p mimic (miR-10a/b mimics) in rescuing diabetes and GI dysmotility in murine models of diabetes. In this study, we elucidated the safety profile of a long-term treatment with miR-10a/b mimics in diabetic mice. **Methods:** Male C57BL6 mice were fed a high-fat, high-sucrose diet (HFHSD) to induce diabetes and treated by five subcutaneous injections of miR-10a/b mimics for a 5-month period. We examined the long-term effect of the miRNA mimics on diabetes and GI dysmotility, including an assessment of cancer risk as well as liver and colon inflammation using cancer and inflammatory biomarkers. **Results:** HFHSD-induced diabetic mice subcutaneously injected with miR-10a/b mimics monthly for 5 months exhibited a marked reduction in fasting blood glucose levels with restoration of insulin and significant weight loss, improved glucose and insulin intolerance, and restored GI transit time. In addition, the miR-10a/b mimic treated diabetic mice showed no indication of risk for cancer development and inflammation induction in the liver, colon, and blood for the 5 months post injections. **Conclusion:** This longitudinal study demonstrates that miR-10a/b mimics, when subcutaneously administered in diabetic mice, effectively alleviate diabetes and GI dysmotility for 5 months with no discernible risk for cancer or inflammation in the liver and colon. The sustained efficacy and favorable safety profiles position miR-10a/b mimics as promising candidates in miRNA-based therapeutics for diabetes and GI dysmotility.

Keywords: miR-10a-5p; miR-10b-5p; diabetes; gastrointestinal dysmotility; cancer; inflammation

1. Introduction

Diabetes, a global health challenge, is increasingly recognized for its association with gastrointestinal (GI) complications, notably GI dysmotility [1–3]. This linkage underscores an intricate interplay between metabolic dysfunction and gut health [2]. Current therapeutic strategies largely focus on symptomatic relief, often falling short in addressing the underlying cellular dysfunctions that contribute to both diabetes and GI dysmotility [4–6]. Thus, there is an imperative need for treatments that target the root causes of these diseases.

Advancements in cellular biology have unveiled the critical role of cell types in maintaining glucose homeostasis and GI functionality [6,7]. More specifically, this includes pancreatic β cells and gastrointestinal pacemaking cells, interstitial cells of Cajal (ICC), each playing a pivotal role in these processes [6,8,9]. Dysfunctions in these cells are key contributors to the onset of diabetes and GI dysmotility, stemming from disruptions at various molecular regulatory levels [10,11]. In this context,

 doi:10.20944/preprints202401.0255.v1

RNA-based therapeutics, particularly microRNAs (miRNAs), emerge as a new therapeutic approach due to their endogenous ability to regulate cellular processes and ability to restore these dysfunctions [12–16].

Our previous research has shed light on the essential role of miR-10a-5p and miR10b-5p (miR-10a/b-5p) in key cell types, including pancreatic β cells and ICC [17,18]. We discovered that miR-10a/b-5p are the most highly expressed in KIT$^+$ ICC in healthy mice and drastically depleted in ICC in diabetic *ob*/*ob* mice and that loss of miR-10b-5p in KIT$^+$ β cells and ICC led to diabetes and GI dysmotility, revealing a novel miR-10a/b-KLF11-KIT pathway that regulates glucose homeostasis and GI motility [17]. In addition, we found that miR-10a-5p mimic and miR-10b-5p mimic (miR-10a/b mimics) intervention in the multiple models of diabetic mice effectively reversed these pathological phenotypes by the restoration of β cells and ICC, highlighting the potential utilization of miR-10a/b mimics in therapeutic applications [17,18].

However, there is a safety concern in the potential therapeutic application of miR-10a/b mimics. Overexpression of miR-10a/b-5p is associated with various types of cancer, raising concerns about its potential oncogenic effect [19–22]. In this study, we conducted a comprehensive assessment of the efficacy and safety profiles of miR-10a/b mimics, monitoring the long-term effect on diabetes and GI dysmotility and the risk for cancer and inflammation using cancer and inflammatory biomarkers in diabetic mice injected with miR-10a/b mimics monthly for a 5-month period.

2. Results

2.1. Long-term treatment of miR-10a/b mimics rescues diabetes in HFHSD-induced diabetic mice without excessive miR-10a/b-5p

To examine the long-term effect of miR-10a/b mimics on diabetes, we used mice that were fed a HFHSD to induce diabetes for 4 months along with mice that were fed a ND. We subcutaneously injected HFHSD-diabetic and ND-healthy mice with miR-10a-5p mimic or miR-10b-5p mimic monthly for 5 months (Figure 1A). HFHSD-fed mice became hyperglycemic and obese compared to those fed with a ND (Figure 1B and C). Notably, the HFHSD-induced diabetic mice showed a marked reduction in fasting blood glucose levels with significant weight loss post-injection (PI) of the miR-10a/b mimics, compared to untreated diabetic mice (Figure 1B and C). Blood glucose levels in HFHSD-induced diabetic mice after miR-10a/b mimic injections were dramatically reduced to normal levels at 1-month PI, which were maintained up to 5-months PI (Figure 1B). Healthy mice injected with miR-10a/b mimics for 5 consecutive times also maintained normal blood glucose levels but did not develop hypoglycemia (Figure 1B). HFHSD-induced diabetic mice after miR-10a/b mimic injections gradually reduced body weight over 5 months while ND-fed healthy mice after miR-10a/b mimic injections maintained normal body weight (Figure 1C).

Preprints (www.preprints.org) | NOT PEER-REVIEWED | Posted: 3 January 2024 doi:10.20944/preprints202401.0255.v1

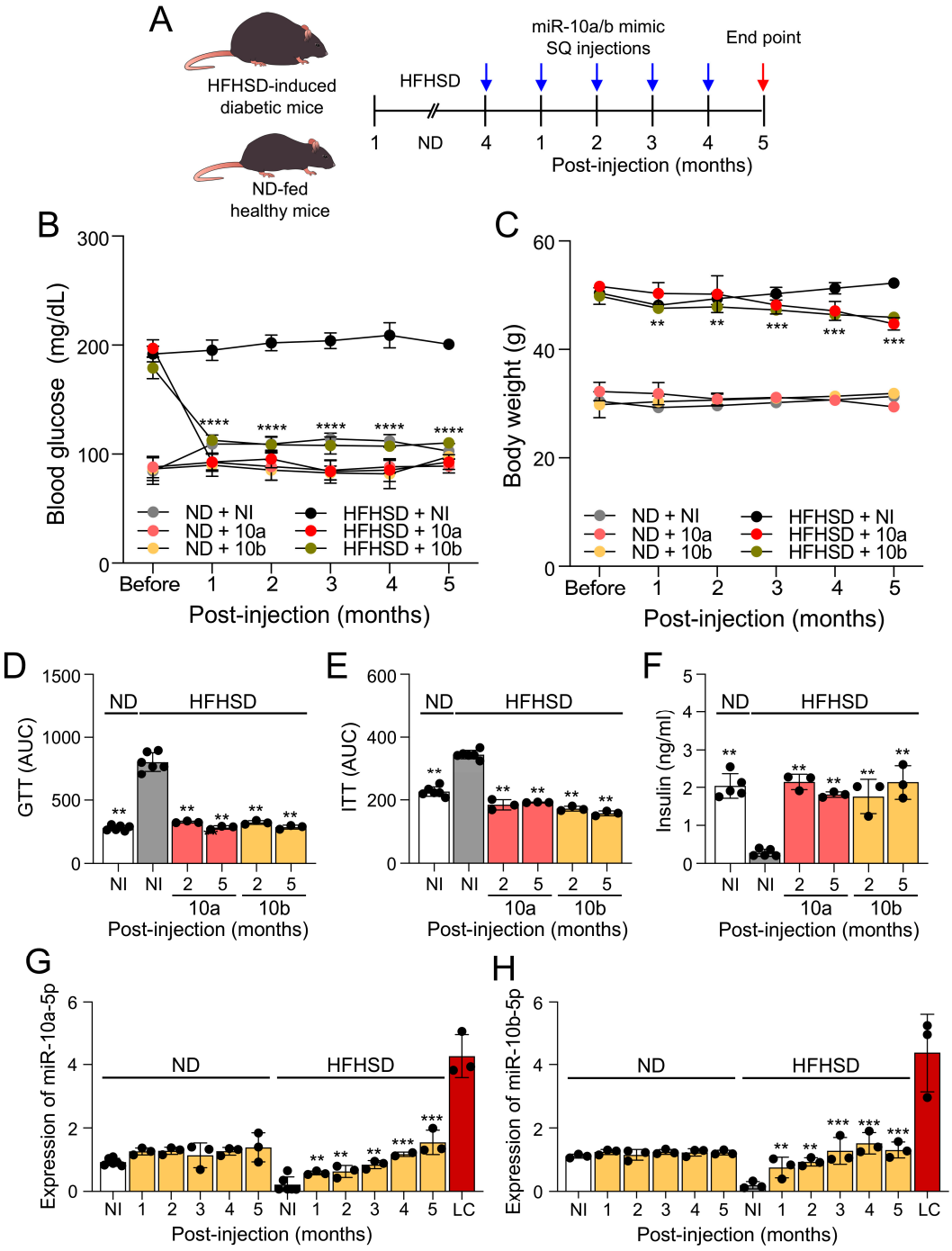

Figure 1. Long-term treatment of miR-10a/b mimics rescues diabetes in high-fat, and high sucrose diet-induced diabetic mice without excessive miR-10a/b-5p. (A) Outline of the study. Male C57BL6 mice were fed a high-fat, high-sucrose diet (HFHSD) or a normal diet (ND) for 4 months and subcutaneously (SQ) injected with miR-10a-5p mimic or miR-10b-5p mimic (miR-10a/b mimics) per each month for a 5-month period. (B) Fasting blood glucose comparison in HFHSD-induced diabetic mice and ND-fed healthy mice injected with miR-10a/b mimics or given no injection (NI) over a 5-month period post-injection (PI). (C) Body weight comparison in HFHSD-induced diabetic and ND-fed healthy mice injected with miR-10a/b mimics or given NI. (D and E) Glucose and insulin tolerance test plots of the area under the curve (AUC) comparison in HFHSD-induced diabetic and ND-fed healthy mice injected with miR-10a/b mimics or given NI. (F) Comparison of insulin levels in plasma

Preprints (www.preprints.org) | NOT PEER-REVIEWED | Posted: 3 January 2024 doi:10.20944/preprints202401.0255.v1

from HFHSD-induced diabetic and ND-fed healthy mice injected with miR-10a/b mimics or given NI. (G, H) Levels of miR-10a-5p and miR-10b-5p in whole blood samples from HFHSD-induced diabetic and ND-fed healthy mice injected with miR-10a/b mimics or given NI, and liver cancer (LC). n=3-6 per condition for each experiment. Error bar indicates mean ± SEM, 2-way analysis of variance [ANOVA]. $^{**}p < 0.01$; $^{***}p < 0.001$; $^{****}p < 0.0001$.

HFHSD-induced diabetic mice exhibited impaired glucose and insulin tolerance, both of which were significantly improved after miR-10a/b mimic injections at 2 months and 5 months PI (Figure 1D and E). Insulin was drastically attenuated in HFHSD-induced diabetic mice but restored to normal levels after miR-10a/b mimic injections at 2 months and 5 months PI (Figure 1F). miR-10a/b-5p levels were substantially reduced in the blood of HFHSD-induced diabetic mice, but were increased to normal levels after miR-10a/b mimic injections as seen in ND-fed healthy mice (Figure 1G and H). However, miR-10a/b mimic injections in ND-fed healthy mice did not further elevate miR-10a/b-5p levels. Monthly miR-10a/b mimic injections in both HFHSD-induced diabetic mice and ND-fed healthy mice did not result in miR-10a/b-5p levels to be elevated to the oncogenic levels of liver cancer. These data demonstrate that subcutaneous miR-10a/b mimic injections in HFHSD-induced diabetic mice effectively rescue the diabetic phenotypes for 5 months without inducing excessive miR-10a/b-5p levels.

2.2. Long-term treatment of miR-10a/b mimics rescues GI dysmotility in HFHSD-induced diabetic mice without indication of risk for colon cancer

To examine the long-term effect of miR-10a/b mimics on GI dysmotility, we performed total GI transit time tests in HFHSD-induced diabetic mice and ND-fed mice. Total GI transit time was noticeably delayed in HFHSD-induced diabetic mice but significantly decreased after miR-10a/b mimic injections at 2 months PI and further decreased to normal GI transit times at 5 months PI as seen in ND-fed healthy mice (Figure 2A). Next, we performed a colorectal cancer screening test in HFHSD-induced diabetic mice and ND-fed healthy mice with five consecutive miR-10a/b mimic injections at 5 months PI using the well-known tumor markers, CEA and CA-19-9 [23], which are used in the diagnosis of colon cancer. Both CEA and CA-19-9 were elevated in the colon cancer blood and cells but not in the blood and colonic tissue from HFHSD-induced diabetic mice and ND-fed healthy mice at 5 months PI (Figure 2B and C). Taken together, the data indicate that the long-term treatment of miR-10a/b mimics can rescue delayed total GI transit in diabetic mice without indication of risk for colon cancer.

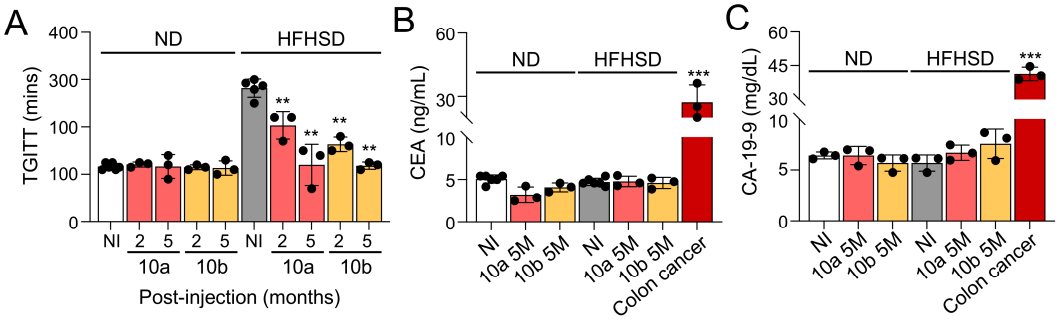

Figure 2. Long-term treatment of miR-10a/b mimics rescues gastrointestinal dysmotility in HFHSD-induced diabetic mice without indication of risk for colon cancer. (A, B) Total gastrointestinal transit time (TGITT) comparison in HFHSD-induced diabetic and ND-fed healthy mice injected with miR-10a/b mimics or given NI.(C) Carcinoembryonic Antigen (CEA) levels comparison in blood samples from HFHSD-induced diabetic and ND-fed healthy mice injected with miR-10a/b mimics or given NI and in colon cancer cells. (D) Carbohydrate antigen 19-9 (CA-19-9) levels comparison in colon tissue from HFHSD-induced diabetic and ND-fed healthy mice injected with miR-10a/b mimics or given NI

Preprints (www.preprints.org) | NOT PEER-REVIEWED | Posted: 3 January 2024 doi:10.20944/preprints202401.0255.v1

and in colon cancer cells. n=3-6 per condition for each experiment. Error bar indicates mean ± SEM, 2-way ANOVA. $^{**}p < 0.01$; $^{***}p < 0.001$.

2.3. Long-term treatment of miR-10a/b mimics in HFHSD-induced diabetic mice indicates no risk for liver cancer

To examine an oncogenic effect of miR-10a/b mimics on liver cancer, we performed a liver cancer screening test in HFHSD-induced diabetic mice and ND-fed healthy mice with five consecutive miR-10a/b mimics injections by using the tumor markers, DCP and AFP, which are widely used to detect hepatocellular carcinoma [24]. Both DCP and AFP levels were elevated in the blood of liver cancer, but not in HFHSD-induced diabetic mice and ND-fed healthy mice with five consecutive miR-10a/b mimics injections at 5 months PI (Figure 3A and B). Similarly, AFP levels were detected in liver cancer tissue at high levels but was detected at lower levels in miR-10a/b mimic injected diabetic mice and healthy mice (Figure 3C). Next, we performed the liver function test, using ALT and AST, which are widely used to detect liver dysfunction and damage [25], in HFHSD-induced diabetic mice and ND-fed healthy mice with five consecutive miR-10a/b mimic injections at 5 months PI. Both ALT and AST were significantly reduced in the blood from HFHSD-induced diabetic mice after miR-10a/b mimic injections at 2 months and 5 months PI (Figure 3D and E). Furthermore, Oil Red O and Picro Sirius staining of liver cross-sections revealed an excessive accumulation of lipids and fibers in the liver tissue of HFHSD-induced diabetic mice, but accumulation was noticeably reduced in the liver tissue of miR-10a mimic injected diabetic mice at 5 months PI (Figure 3F). miR-10b mimic injected diabetic mice also showed a marked decrease of lipids and fibers although the reduction of lipids was less notable compared to use of the miR-10a mimic. These findings imply that the long-term treatment of miR-10a/b mimics can rescue fatty and fibrous liver or liver dysfunction in diabetic mice without indication of risk for liver cancer.

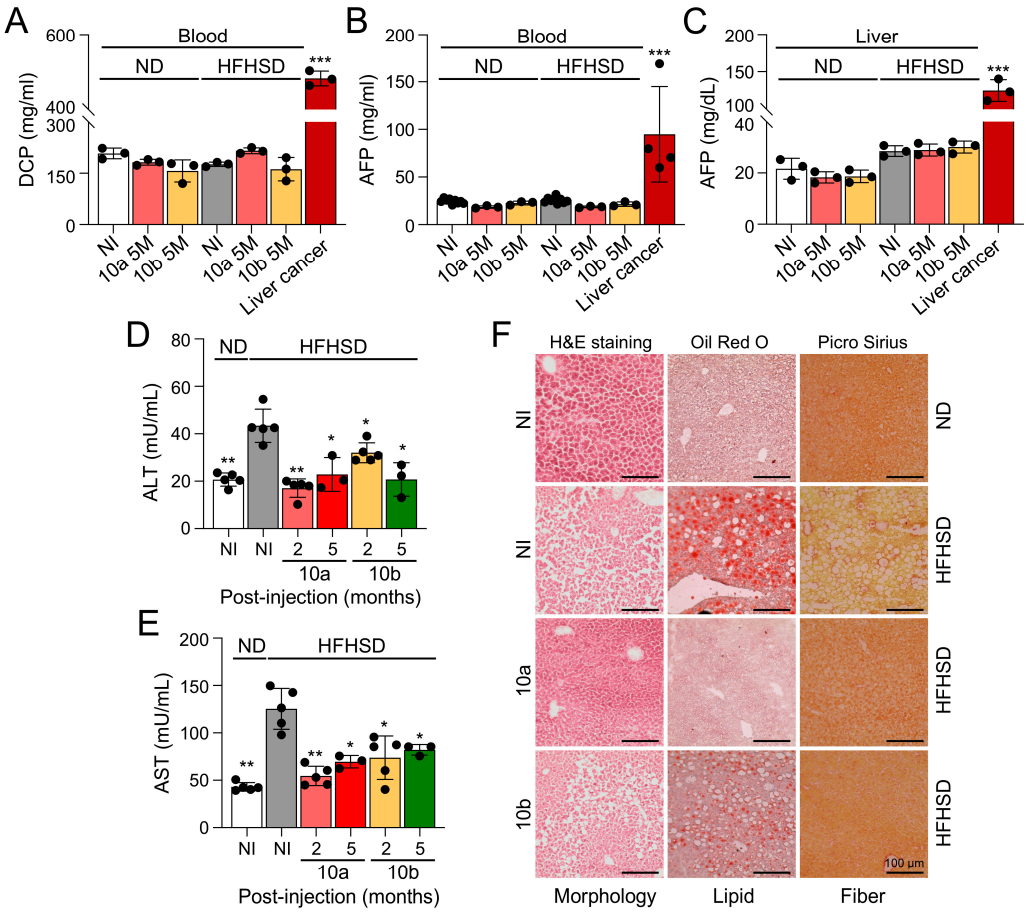

 doi:10.20944/preprints202401.0255.v1

Figure 3. Long-term treatment of miR-10a/b mimics in HFHSD-induced diabetic mice indicates no risk for liver cancer. (A) Comparison of Des-Gamma-Carboxy Prothrombin (DCP) levels in blood samples from HFHSD-induced diabetic and ND-fed healthy mice injected with miR-10a/b mimics or given NI and mice with liver cancer. (B) Comparison of Alpha-fetoprotein (AFP) levels in blood samples from HFHSD-induced diabetic and ND-fed healthy mice injected with miR-10a/b mimics or given NI and mice with liver cancer. (C) Comparison of Alpha-fetoprotein (AFP) levels in liver tissue from HFHSD-induced diabetic and ND-fed healthy mice injected with miR-10a/b mimics or given NI and in liver cancer tissue. (D and E) Comparison of liver function tests (ALT and AST levels) in blood samples from HFHSD-induced diabetic and ND-fed healthy mice injected with miR-10a/b mimics or given NI. (F) Liver cryostat sections of H& E, Oil Red O, and Picro Sirius for comparison of morphology, lipid droplets, and fiber content in the liver tissue of HFHSD-induced diabetic and ND-fed healthy mice injected with miR-10a/b mimics or given NI. Scale bars are 50 μm. n=3 per condition for each experiment. Error bar indicates mean ± SEM, 2-way ANOVA. *$p < 0.05$; **$p < 0.01$; ***$p < 0.001$.

2.4. Long-term treatment of miR-10a/b mimics in HFHSD-induced diabetic mice indicates no risk for inflammation in colon and liver

To provide a comprehensive assessment of the safety profile of mice treated with miR-10a/b mimics, we further assessed inflammation in the colon and liver by measuring anti-/pro-inflammatory cytokines in miR-10a/b mimic injected diabetic mice.

Both anti-inflammatory cytokines, interleukin 10 (IL-10) and transforming growth factor-beta1 (TGF-β1), were noticeably decreased in the colon of HFHSD-induced diabetic mice, compared to ND-fed healthy mice, but were significantly restored in miR-10a/b mimic injected diabetic mice 5 months PI (Figure 4A and B). In contrast, both pro-inflammatory cytokines, IL-6 and tumor necrosis factor-alpha (TNF-α), were markedly increased in the colon of HFHSD-induced diabetic mice, compared to ND-fed healthy mice but were significantly decreased in the colon of miR-10a/b mimic injected diabetic mice 5 months PI (Figure 4C and D). In addition, IL-6 was significantly reduced in the blood and liver of diabetic mice after miR-10a/b mimic injections at 2 months and 5 months PI (Figure 4E). These inflammation tests in the colon, liver, and blood confirm that the long-term treatment of miR-10a/b mimics in HFHSD-induced diabetic mice indicates no risk for inflammation in the colon and liver.

Preprints (www.preprints.org) | NOT PEER-REVIEWED | Posted: 3 January 2024 doi:10.20944/preprints202401.0255.v1

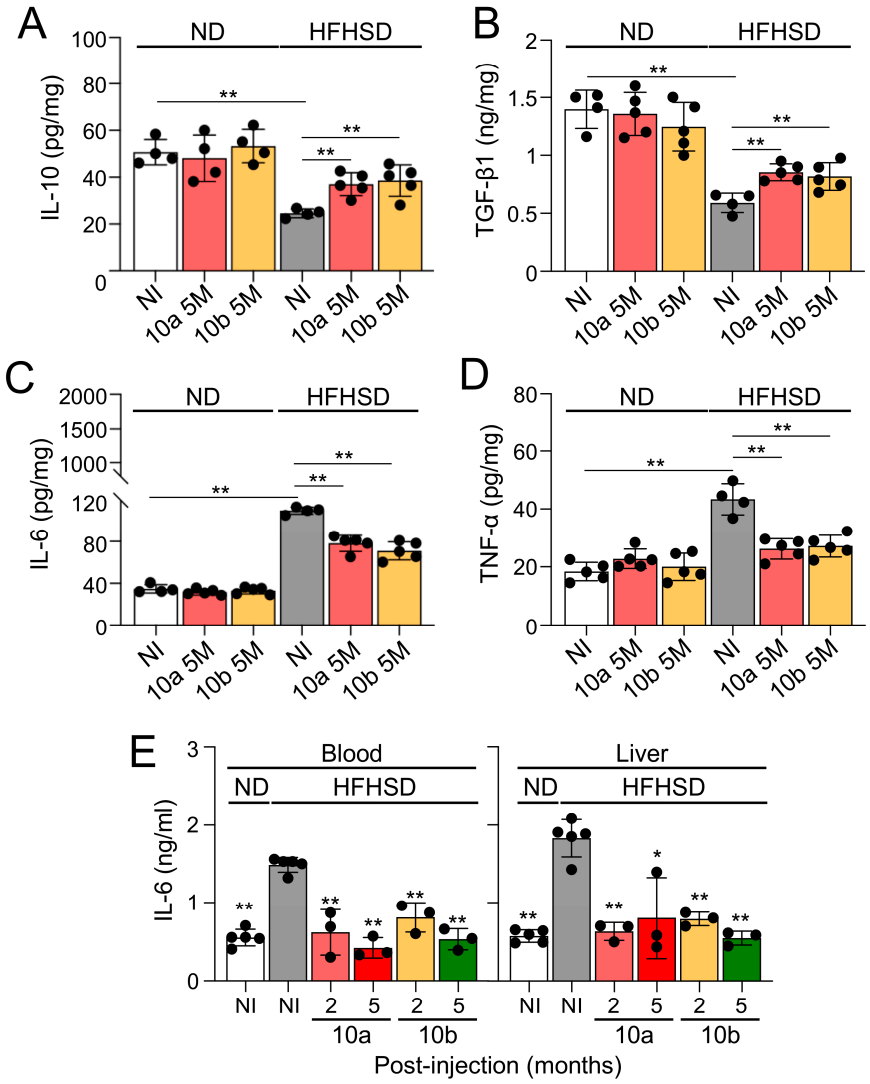

Figure 4. Long-term treatment of miR-10a/b mimics in HFHSD-induced diabetic mice indicates no risk for inflammation in the colon and liver. (A) Comparison of interleukin 10 (IL-10) levels in colon tissue from HFHSD-induced diabetic and ND-fed healthy mice injected with miR-10a/b mimics or given NI (B) Comparison of transforming growth factor beta (TGF-β) levels in colon tissue from HFHSD-induced diabetic and ND-fed healthy mice injected with miR-10a/b mimics or given NI (C) Comparison of interleukin (IL-6) levels in colon tissue from HFHSD-induced diabetic and ND-fed healthy mice injected with miR-10a/b mimics or given NI (D) Comparison of tumor necrosis factor alpha (TNF-α) levels in colon tissue from HFHSD-induced diabetic and ND-fed healthy mice injected with miR-10a/b mimics or given NI. (E) Comparison of IL-6 levels in blood and liver tissue from HFHSD-induced diabetic and ND-fed healthy mice injected with miR-10a/b mimics or given NI. n=4-5 per condition for each experiment. Error bar indicates mean ± SEM, 2-way ANOVA. *$p < 0.05$; **$p < 0.01$.

3. Discussion

This study has explored the therapeutic potential and safety of miR-10a/b mimics in treating diabetes and GI dysmotility without the possible risk for cancer and inflammation. Our results indicate that the long-term treatment of HFHSD-induced diabetic mice treated with miR-10a/b mimics can effectively rescue both diabetes and GI dysmotility with no indication for cancer development and inflammation induction. These efficacy and safety data are consistent with our

 doi:10.20944/preprints202401.0255.v1

previous studies [17,18] that highlighted the pivotal role of miR-10a/b-5p in regulating glucose homeostasis and GI motility as well as the promising efficacy of miR-10a/b mimics in reversing diabetes and GI dysmotility with no indication of risk for cancer development.

In our previous study, we tested the safety of miR-10b-5p mimic at two therapeutic dosages of 500 ng/g injected in healthy mice and observed no indication of cancer development in the mice over an extended period of one year [17]. We further demonstrated that a single injection of the miR-10b-5p mimic into HFHSD-fed diabetic mice restored miR-10b-5p in blood to approximately 40%–60% of normal, healthy levels but not to the excessively elevated levels reported in cancers [19,20] and in liver cancer that we tested in this study [17].

An essential aspect of the current study was assessing the extended safety profile of a long-term miR-10a/b mimic treatment for diabetic mice, particularly the risk pertaining to for cancer and inflammation. Our longitudinal study, encompassing blood- and tissue-based cancer biomarker screening, showed no indication of risk for cancer development and inflammation induction in the liver, colon, and blood. Notably, although overexpression of miR-10a/b-5p has been linked to cancer in various contexts [19–21], our study indicates that the five monthly doses of 500 ng/g of miR-10a/b mimics injected in diabetic mice are safe as they do not reach the excessive oncogenic levels of miR-10a/b-5p were not reached.

miR-10a/b-5p are bifunctional in cancer as they function as both tumor suppressors and oncogenes, inhibiting or promoting cancer development and progression, depending on the cellular contexts and the genes they target [26,27]. Overexpression of miR-10a/b-5p is associated with various types of cancer, contributing to enhance cell proliferation and migration [19–21]. However, it is also well-documented that miR-10a/b-5p are downregulated in certain cancer and inhibit tumorigenicity [28–31] . miR-10a/b-5p have both oncogenic and tumor-suppressive roles in gastric cancer [27], colorectal cancer [32], breast cancer [33], and gynecological malignancies [26]. The dual function of miR-10a/b-5p is dependent on their target genes. miR-10a/b-5p are encoded within the Hox clusters of developmental regulators and regulate the translation of Hox transcripts [34]. HOX genes have both tumor suppressor and pro-oncogenic activities [35]. miR-10a/b-5p also target and suppress the protein translation of Krüppel-like factor 11 (KLF11), which induces apoptosis or cell cycle arrest [17,36]. KLF11 also has a dual function in cell growth and cancer as a tumor suppressor and a tumor promoter [36]. We previously found that miR-10a/b-5p induce the growth of ICC and pancreatic β cells by targeting KLF11, which negatively regulates expression of KIT and INS [17]. KIT functions as a proto-oncogene via its kinase activity as well as a tumor suppressor via its receptor activity [37]. KIT is required for the normal growth and differentiation of ICC, but excessive KIT triggers gastrointestinal stromal tumor [38].

Our current study observed a restoration of colonic and liver inflammatory cytokines in mice treated with miR-10a/b mimics, suggesting an anti-inflammatory role. This observation aligns with previous studies that have confirmed the anti-inflammatory function of miR-10a/b-5p in both murine and human gut inflammatory conditions [39–44]. Specifically, murine studies have shown that a deficiency of miR-10a/b-5 can exacerbate dextran sodium sulfate-induced inflammatory responses by impairing intestinal barrier function [39]. Additionally, studies found downregulation of miR-10a/b-5p in patients with inflammatory bowel disease, particularly in patients with colitis [42,44]. Furthermore, previous studies have demonstrated that miR-10a/b-5p might regulate macrophage functions, facilitating a transition in their phenotypes from pro-inflammatory to anti-inflammatory [45,46]. The ability of miR-10a/b-5p to alleviate these inflammatory phenotypes and reduce inflammation holds significant promise for clinical applications, especially in treating patients with both diabetes and GI dysmotility.

The role of miR-10a/b extends beyond the mere regulation of pancreatic β cells and ICC function; they are pivotal in reprogramming intestinal epithelial cells, which is crucial for GI homeostasis and metabolic health. Our previous study revealed that global *mir-10b* KO mice displayed impaired intestinal barrier function, characterized by a disorganized epithelial barrier, increased gut permeability, and reduced expression of ZO-1 [18]. Intervention with a miR-10b mimic in these mice rescued the hyperglycemic, GI dysmotility and the leaky gut phenotype through remodeling

 doi:10.20944/preprints202401.0255.v1

epithelial cells, thereby maintaining GI homeostasis and metabolic health [18]. Our findings contribute to this understanding by demonstrating how miR-10a/b mimics treatment may beneficially restore GI pathophysiology associated with diabetic conditions.

The implications of our study are far-reaching, highlighting the potential of miR-10a/b mimics as a therapeutic potential for disorders associated with the loss of these miRNAs. By targeting the underlying causes (dysfunction or loss of pancreatic β cells and ICC) of diabetes and GI dysmotility, miR-10a/b mimics offer a more comprehensive approach compared to current treatments that focus solely on symptomatic treatment and temporary relief. Furthermore, we have explored the therapeutic potential of miR-10a/b mimics delivered via a subcutaneous injection in mice. This subcutaneous method aligns with the translational approach to diabetes treatment, as current diabetic medications, such as GLP1 receptor agonists (liraglutide and semaglutide), also use subcutaneous injections [47,48]. Our findings, demonstrating the efficacy of subcutaneously delivered miR-10a/b mimics in lowering blood glucose levels and body weight, mirror the results from our previous study using miR-10a/b mimics that are administered intraperitoneally. This study paves the way for further research, especially in optimizing miR-10a/b mimic dosages and frequencies, and investigating their long-term effects on various metabolic conditions including obesity and fatty liver disease. Future studies could also explore the applicability of these potential miR-10a/b mimics in other inflammatory diseases where they may alleviate the disease conditions.

While our findings are promising, it is important to acknowledge the limitations of our study. The research was conducted in a diet-induced murine model, and thus, the translational applicability to human patients requires further investigation. Additionally, although we observed no cancer and inflammation risk in our HFHSD-induced diabetic mice with multiple injections of miR-10a/b mimics, long-term studies in the murine cancer models are essential to fully understand the oncogenic potential of miR-10a/b-5p.

In conclusion, our study provides compelling evidence for the therapeutic potential of miR-10a/b mimics in treating diabetes and gut dysmotility. The safety profile, alongside the observed efficacy, positions miR-10a/b mimics as promising candidates to treat diabetes and GI dysmotility in the realm of RNA-based therapeutics. As we continue to unravel the complexities of the miR-10a/b functions, miR-10a/b mimics offer hope for more effective treatments using β cells and ICC-targeted approaches to combating diabetes and GI dysmotility.

4. Materials and Methods

4.1. Mice

C57BL6 male mice were obtained from Jackson Laboratory. The Institutional Animal Care and Use Committee at the University of Nevada, Reno (UNR) approved all experimental procedures. The colony of mice included in this study were housed in a centralized animal facility at the UNR Animal Resources. UNR is fully accredited by the American Association for Accreditation of Laboratory Animal Care International. Animals were air-freighted to UNR, where they were housed in the transgenic facility at the UNR School of Medicine. All mice were housed under pathogen-free conditions on a 12-hour light/dark cycle with food and water *ad libitum*. Mice were euthanized by inhaling CO2, followed by cervical dislocation. A ventral midline incision was made, and the whole GI tract was carefully excised. These procedures were in accordance with National Institutes of Health guidelines for the care and use of laboratory animals.

4.2. Diet

The mice were fed one of two purified Teklad diets, *ad libitum*, from ENVIGO: a purified control diet (TD.08806) containing 20.5% kcal from protein, 10.5% kcal from fat, and 69.1% kcal from carbohydrates; or a high-fat, high-sucrose diet (representative western diet) (TD.130784) containing 14.7% kcal from protein, 44.6% kcal from fat, and 40.7% kcal from carbohydrates.

 doi:10.20944/preprints202401.0255.v1

4.3. miR-10a/b mimics intervention

Subcutaneous (SQ) injection of 500 ng/g of the miR-10a/b mimics (a chemically modified double-stranded RNA molecule that mimics endogenous miR-10a/b upregulates miRNA activity) was administered to male mice. *In vivo-jetPEI* (Polyplus-transfection) was used as the delivery agent. *In vivo-jetPEI*/miRNA complexes were prepared according to the manufacturer's protocol, as previously described [17]. SQ injections were performed on mice using complexes equilibrated at room temperature.

4.4. Metabolic procedures

Body weight and 6-hour fasting blood glucose measurements were monitored monthly. A glucose tolerance test (GTT) was performed by measuring the 6-hour fasting blood glucose levels as well as blood glucose levels at 15-, 30-, 60-, 90-, and 120-minutes post-glucose injection (2g/kg body weight) [17]. An insulin tolerance test (ITT) was performed by measuring the 6-hour fasting blood glucose levels as well as blood glucose levels at 30-, 60-, 90-, and 120-minutes post-insulin glargine Lantus (0.75 IU/kg) injection [17]. Area under the curve analysis for both GTT and ITT was performed using GraphPad Prism 9 software.

4.5. Total gastrointestinal transit time test

Total gastrointestinal transit time (TGITT) test was performed on mice fasted overnight. The mice were orally gavaged with 0.1 mL of a semiliquid solution containing 5% Evans blue in 0.9% NaCl and 0.5% methylcellulose. The mice were then monitored every 10 minutes until a fecal pellet containing the Evans blue solution was expelled. TGITT was calculated as the time between the intragastric gavage of the dye and the visualization of the first blue fecal pellet [17].

4.6. Reverse Transcription Quantitative Polymerase Chain Reaction

Total RNAs were isolated from blood samples using the mirVana miRNA Isolation Kit (Ambion) as previously described [17]. RNA quality and quantity were evaluated using a Nanodrop 2000 Spectrophotometer (Thermo Fisher Scientific), then total RNAs were reverse transcribed into complementary DNA (cDNA) using the TaqMan™ MicroRNA Reverse Transcription Kit (Waltham, MA, USA). The following TaqMan Advanced MicroRNA Assay probes were used: hsa-miR-10a-5p/mmu-miR-10a-5p (Gene ID: MI0000266), and mmu-U6 (Gene ID: NR_004394). A standard qPCR protocol was followed on qTOWER3 84 (Analytik Jena, Germany). The comparative cycle threshold method was used to compare relative transcription levels. The transcription level of each miRNA was estimated as the relative fold-change over the control U6 genes. All samples were run in triplicate for each assay.

4.7. Enzyme-Linked Immunosorbent Assay

Des-gamma-carboxy prothrombin (DCP), Alpha-fetoprotein (AFP), Carcinoembryonic Antigen (CEA), Carbohydrate antigen 19-9 (CA-19-9), IL-10, TGF-β, IL-6, TNF-α, and insulin measurements were gathered from mouse blood or tissue. Blood was collected by penetrating the retro-orbital sinus of the mice. The blood was stored in a vial containing EDTA to prevent blood clotting. The blood was then spun down at 15000 rpm for 15 minutes at 4°C in order to collect the plasma. Plasma was collected and stored at -80°C. Liver and colonic tissues were homogenized in radioimmunoprecipitation assay (RIPA) buffer using a Bullet Blender. The homogenate was then centrifuged at 12,000 rpm for 5 minutes at 4°C. The supernatant was then collected and stored at -80°C. A detergent compatible Bradford assay was then performed to measure the protein concentration of each sample. Enzyme-linked immunosorbent Assays (ELISAs) were performed on plasma and/or tissue samples using ELISA kits DCP, AFP, CEA, CA-19-9, IL-10, TGF-β, IL-6, TNF-α, and insulin. All kits were used according to the manufacturer's protocol.

4.8. Immunohistochemical and confocal microscopy analysis

Murine liver tissue was analyzed through cryostat sectioned staining and confocal microscopy. Liver tissues were dissected in Krebs buffer (125.35 mmol/L NaCl, 5.9 mmol/L KCl, 1.2 mmol/L $NaHPO_4$, 15.5 mmol/L $NaHCO_3$, 1.2 mmol/ L $MgCl_2$, 11.5 mmol/L D-glucose, and 2.5 mmol/L $CaCl_2$). Fresh liver tissue was fixed in 4% paraformaldehyde at 4°C for 20 minutes, followed by overnight incubation in 1 X Tris-buffered saline (TBS) at 4°C. Dehydration was performed in 20% sucrose in TBS at 4°C. Tissue was trimmed and placed in 1:1 optimum cutting temperature (OCT)/20% sucrose in TBS and flash frozen by liquid nitrogen. Then, 8 mm-thickness cryosections were used for immunohistochemistry staining experiments. The section was blocked with 0.5% Triton X-114, 4% skim milk in TBS for 1 hour at room temperature, rinsed with TBS twice for 10 minutes each, and then incubated with anti-Alpha fetoprotein (rabbit, 1:100, Proteintech, Rosemont, IL, USA) for 48 hours on a rocker at 4°C. The slide was rinsed with TBS twice for 10 minutes each and then incubated with 594-anti-rabbit (Jackson ImmunoResearch) for 2 hours at room temperature. The specimen was rinsed with 1X TBS 3 times for 10 minutes each, dried, and mounted (mounting medium with 4', 6-diamidino-2-phenylindole (DAPI). An Olympus Fluoview FV1000 confocal laser scanning microscope was used for all imaging analysis.

4.9. Hematoxylin and eosin, Oil Red O, and Picro Sirius staining

Liver cryostat sections were stained with Hematoxylin and Eosin Y solution (ab245880) or Picro-Sirius Red Solution (ab150681) according to the manufacturer's protocol. For Oil Red O staining, liver Cryostat sectioned slides were exposed to pure propylene glycol, then moved to 0.5% Oil Red O solution at 60°C, followed by soaking in 85% propylene glycol. The slides were then rinsed and counterstained with hematoxylin, rinsed with water, then mounted with aqueous mounting reagent, and allowed to cure. The slides were imaged with a Keyence BZ-x710 brightfield microscope.

4.10. Statistical analyses

The experimental data are shown as the mean ± SEM. Two-tailed unpaired Student's t-test, area under the curve calculations, and one-way or two-way analysis of variance (ANOVA) were used for all mouse experiments using GraphPad Prism 9 software. For all tests, p-values less than 0.05 were considered statistically significant.

Author Contributions: Conceptualization: R.S., S.E.H., S.R.; methodology: R.S., S.E.H.; investigation: R.S., S.E.H., H.S.P., S.D., H.C., G.B., T.Y.Y.; writing: R.S., S.H., S.R.; and funding acquisition: S.R.

Funding: Research was supported by RosVivo Therapeutics (AWD-01-00003158 to S.R.) and NIDDK (DK103055 to S.R.).

Institutional Review Board Statement: *C57BL6* male mice were obtained from Jackson Laboratory. The Institutional Animal Care and Use Committee at the University of Nevada, Reno (UNR) approved all experimental procedures.

Data Availability Statement: The data supporting this study's findings are available on request from the corresponding author.

Acknowledgments: We would like to thank Benjamin J Weigler, D.V.M., and Walt Mandeville, D.V.M. for their excellent animal services provided to the mice.

Conflicts of Interest: This author discloses the following: S.R. and the University of Nevada Reno Office of Technology Transfer (serial no. 62/837,988, filed April 24, 2019) have published a PCT International Patent WO/2020/219872 entitled "Methods and compositions of miR-10 mimics and targets thereof." S.R. is an employee and a member of the board of directors of RosVivo Therapeutics. R.S. and S.E.H. are members of the board of directors of RosVivo Therapeutics.

References

1. Ogurtsova, K.; Guariguata, L.; Barengo, N.C.; Ruiz, P.L.; Sacre, J.W.; Karuranga, S.; Sun, H.; Boyko, E.J.; Magliano, D.J. IDF diabetes Atlas: Global estimates of undiagnosed diabetes in adults for 2021. *Diabetes Res Clin Pract* **2022**, *183*, 109118, doi:10.1016/j.diabres.2021.109118.

2. Singh, R.; Zogg, H.; Wei, L.; Bartlett, A.; Ghoshal, U.C.; Rajender, S.; Ro, S. Gut Microbial Dysbiosis in the Pathogenesis of Gastrointestinal Dysmotility and Metabolic Disorders. *J Neurogastroenterol Motil* **2021**, *27*, 19-34, doi:10.5056/jnm20149.
3. Camilleri, M.; Chedid, V.; Ford, A.C.; Haruma, K.; Horowitz, M.; Jones, K.L.; Low, P.A.; Park, S.Y.; Parkman, H.P.; Stanghellini, V. Gastroparesis. *Nat Rev Dis Primers* **2018**, *4*, 41, doi:10.1038/s41572-018-0038-z.
4. Camilleri, M.; Kuo, B.; Nguyen, L.; Vaughn, V.M.; Petrey, J.; Greer, K.; Yadlapati, R.; Abell, T.L. ACG Clinical Guideline: Gastroparesis. *Am J Gastroenterol* **2022**, *117*, 1197-1220, doi:10.14309/ajg.0000000000001874.
5. Singh, R.; Zogg, H.; Ghoshal, U.C.; Ro, S. Current Treatment Options and Therapeutic Insights for Gastrointestinal Dysmotility and Functional Gastrointestinal Disorders. *Front Pharmacol* **2022**, *13*, 808195, doi:10.3389/fphar.2022.808195.
6. Eizirik, D.L.; Pasquali, L.; Cnop, M. Pancreatic beta-cells in type 1 and type 2 diabetes mellitus: different pathways to failure. *Nat Rev Endocrinol* **2020**, *16*, 349-362, doi:10.1038/s41574-020-0355-7.
7. Sanders, K.M.; Ward, S.M.; Koh, S.D. Interstitial cells: regulators of smooth muscle function. *Physiol Rev* **2014**, *94*, 859-907, doi:10.1152/physrev.00037.2013.
8. Ro, S.; Park, C.; Jin, J.; Zheng, H.; Blair, P.J.; Redelman, D.; Ward, S.M.; Yan, W.; Sanders, K.M. A model to study the phenotypic changes of interstitial cells of Cajal in gastrointestinal diseases. *Gastroenterology* **2010**, *138*, 1068-1078 e1061-1062, doi:10.1053/j.gastro.2009.11.007.
9. Hrovatin, K.; Bastidas-Ponce, A.; Bakhti, M.; Zappia, L.; Buttner, M.; Salinno, C.; Sterr, M.; Bottcher, A.; Migliorini, A.; Lickert, H., et al. Delineating mouse beta-cell identity during lifetime and in diabetes with a single cell atlas. *Nat Metab* **2023**, *5*, 1615-1637, doi:10.1038/s42255-023-00876-x.
10. Hudish, L.I.; Reusch, J.E.; Sussel, L. beta Cell dysfunction during progression of metabolic syndrome to type 2 diabetes. *J Clin Invest* **2019**, *129*, 4001-4008, doi:10.1172/JCI129188.
11. Grover, M.; Bernard, C.E.; Pasricha, P.J.; Lurken, M.S.; Faussone-Pellegrini, M.S.; Smyrk, T.C.; Parkman, H.P.; Abell, T.L.; Snape, W.J.; Hasler, W.L., et al. Clinical-histological associations in gastroparesis: results from the Gastroparesis Clinical Research Consortium. *Neurogastroenterol Motil* **2012**, *24*, 531-539, e249, doi:10.1111/j.1365-2982.2012.01894.x.
12. Singh, R.; Zogg, H.; Ro, S. Role of microRNAs in Disorders of Gut-Brain Interactions: Clinical Insights and Therapeutic Alternatives. *J Pers Med* **2021**, *11*, doi:10.3390/jpm11101021.
13. Zogg, H.; Singh, R.; Ro, S. Current Advances in RNA Therapeutics for Human Diseases. *Int J Mol Sci* **2022**, *23*, doi:10.3390/ijms23052736.
14. Poy, M.N.; Eliasson, L.; Krutzfeldt, J.; Kuwajima, S.; Ma, X.; Macdonald, P.E.; Pfeffer, S.; Tuschl, T.; Rajewsky, N.; Rorsman, P., et al. A pancreatic islet-specific microRNA regulates insulin secretion. *Nature* **2004**, *432*, 226-230, doi:10.1038/nature03076.
15. Belgardt, B.F.; Ahmed, K.; Spranger, M.; Latreille, M.; Denzler, R.; Kondratiuk, N.; von Meyenn, F.; Villena, F.N.; Herrmanns, K.; Bosco, D., et al. The microRNA-200 family regulates pancreatic beta cell survival in type 2 diabetes. *Nat Med* **2015**, *21*, 619-627, doi:10.1038/nm.3862.
16. Buck, A.H. Cells choose their words wisely. *Cell* **2022**, *185*, 1114-1116, doi:10.1016/j.cell.2022.03.010.
17. Singh, R.; Ha, S.E.; Wei, L.; Jin, B.; Zogg, H.; Poudrier, S.M.; Jorgensen, B.G.; Park, C.; Ronkon, C.F.; Bartlett, A., et al. miR-10b-5p Rescues Diabetes and Gastrointestinal Dysmotility. *Gastroenterology* **2021**, *160*, 1662-1678 e1618, doi:10.1053/j.gastro.2020.12.062.
18. Zogg, H.; Singh, R.; Ha, S.E.; Wang, Z.; Jin, B.; Ha, M.; Dafinone, M.; Batalon, T.; Hoberg, N.; Poudrier, S., et al. miR-10b-5p rescues leaky gut linked with gastrointestinal dysmotility and diabetes. *United European Gastroenterol J* **2023**, *11*, 750-766, doi:10.1002/ueg2.12463.
19. Sheedy, P.; Medarova, Z. The fundamental role of miR-10b in metastatic cancer. *Am J Cancer Res* **2018**, *8*, 1674-1688.
20. Guessous, F.; Alvarado-Velez, M.; Marcinkiewicz, L.; Zhang, Y.; Kim, J.; Heister, S.; Kefas, B.; Godlewski, J.; Schiff, D.; Purow, B., et al. Oncogenic effects of miR-10b in glioblastoma stem cells. *J Neurooncol* **2013**, *112*, 153-163, doi:10.1007/s11060-013-1047-0.
21. Tu, J.; Cheung, H.H.; Lu, G.; Chen, Z.; Chan, W.Y. MicroRNA-10a promotes granulosa cells tumor development via PTEN-AKT/Wnt regulatory axis. *Cell Death Dis* **2018**, *9*, 1076, doi:10.1038/s41419-018-1117-5.
22. Xiong, G.; Huang, H.; Feng, M.; Yang, G.; Zheng, S.; You, L.; Zheng, L.; Hu, Y.; Zhang, T.; Zhao, Y. MiR-10a-5p targets TFAP2C to promote gemcitabine resistance in pancreatic ductal adenocarcinoma. *J Exp Clin Cancer Res* **2018**, *37*, 76, doi:10.1186/s13046-018-0739-x.
23. Vukobrat-Bijedic, Z.; Husic-Selimovic, A.; Sofic, A.; Bijedic, N.; Bjelogrlic, I.; Gogov, B.; Mehmedovic, A. Cancer Antigens (CEA and CA 19-9) as Markers of Advanced Stage of Colorectal Carcinoma. *Med Arch* **2013**, *67*, 397-401, doi:10.5455/medarh.2013.67.397-401.
24. Zhao, Y.J.; Ju, Q.; Li, G.C. Tumor markers for hepatocellular carcinoma. *Mol Clin Oncol* **2013**, *1*, 593-598, doi:10.3892/mco.2013.119.

25. Kalas, M.A.; Chavez, L.; Leon, M.; Taweesedt, P.T.; Surani, S. Abnormal liver enzymes: A review for clinicians. *World J Hepatol* **2021**, *13*, 1688-1698, doi:10.4254/wjh.v13.i11.1688.
26. Li, C.; Zhu, X.; Lv, X.; Han, X.; Xu, Y.; Huang, J.; Chen, X.; Yu, Z. Recent Updates on the Role of the MicroRNA-10 Family in Gynecological Malignancies. *J Oncol* **2022**, *2022*, 1544648, doi:10.1155/2022/1544648.
27. Liu, F.; Shi, Y.; Liu, Z.; Li, Z.; Xu, W. The emerging role of miR-10 family in gastric cancer. *Cell Cycle* **2021**, *20*, 1468-1476, doi:10.1080/15384101.2021.1949840.
28. Gao, L.; Yang, X.; Zhang, H.; Yu, M.; Long, J.; Yang, T. Inhibition of miR-10a-5p suppresses cholangiocarcinoma cell growth through downregulation of Akt pathway. *Onco Targets Ther* **2018**, *11*, 6981-6994, doi:10.2147/OTT.S182225.
29. Shen, D.; Zhao, H.Y.; Gu, A.D.; Wu, Y.W.; Weng, Y.H.; Li, S.J.; Song, J.Y.; Gu, X.F.; Qiu, J.; Zhao, W. miRNA-10a-5p inhibits cell metastasis in hepatocellular carcinoma via targeting SKA1. *Kaohsiung J Med Sci* **2021**, *37*, 784-794, doi:10.1002/kjm2.12392.
30. Hou, R.; Wang, D.; Lu, J. MicroRNA-10b inhibits proliferation, migration and invasion in cervical cancer cells via direct targeting of insulin-like growth factor-1 receptor. *Oncol Lett* **2017**, *13*, 5009-5015, doi:10.3892/ol.2017.6033.
31. Nagy, Z.B.; Wichmann, B.; Kalmar, A.; Galamb, O.; Bartak, B.K.; Spisak, S.; Tulassay, Z.; Molnar, B. Colorectal adenoma and carcinoma specific miRNA profiles in biopsy and their expression in plasma specimens. *Clin Epigenetics* **2017**, *9*, 22, doi:10.1186/s13148-016-0305-3.
32. Liu, Y.; Zhang, Y.; Wu, H.; Li, Y.; Zhang, Y.; Liu, M.; Li, X.; Tang, H. miR-10a suppresses colorectal cancer metastasis by modulating the epithelial-to-mesenchymal transition and anoikis. *Cell Death Dis* **2017**, *8*, e2739, doi:10.1038/cddis.2017.61.
33. Ke, K.; Lou, T. MicroRNA-10a suppresses breast cancer progression via PI3K/Akt/mTOR pathway. *Oncol Lett* **2017**, *14*, 5994-6000, doi:10.3892/ol.2017.6930.
34. Lund, A.H. miR-10 in development and cancer. *Cell Death Differ* **2010**, *17*, 209-214, doi:10.1038/cdd.2009.58.
35. Morgan, R.; Hunter, K.; Pandha, H.S. Downstream of the HOX genes: Explaining conflicting tumour suppressor and oncogenic functions in cancer. *Int J Cancer* **2022**, *150*, 1919-1932, doi:10.1002/ijc.33949.
36. Lin, L.; Mahner, S.; Jeschke, U.; Hester, A. The Distinct Roles of Transcriptional Factor KLF11 in Normal Cell Growth Regulation and Cancer as a Mediator of TGF-beta Signaling Pathway. *Int J Mol Sci* **2020**, *21*, doi:10.3390/ijms21082928.
37. Wang, H.; Boussouar, A.; Mazelin, L.; Tauszig-Delamasure, S.; Sun, Y.; Goldschneider, D.; Paradisi, A.; Mehlen, P. The Proto-oncogene c-Kit Inhibits Tumor Growth by Behaving as a Dependence Receptor. *Mol Cell* **2018**, *72*, 413-425 e415, doi:10.1016/j.molcel.2018.08.040.
38. Ke, H.; Kazi, J.U.; Zhao, H.; Sun, J. Germline mutations of KIT in gastrointestinal stromal tumor (GIST) and mastocytosis. *Cell Biosci* **2016**, *6*, 55, doi:10.1186/s13578-016-0120-8.
39. Zhao, K.; Wang, C.; Liu, Y.; Li, Y.; Hui, T.; Wang, G.; Zhang, X.; Xue, X.; Kang, J.; Feng, G. Deficiency of microRNA-10b promotes DSS-induced inflammatory response via impairing intestinal barrier function. *Biochem Biophys Res Commun* **2022**, *636*, 48-54, doi:10.1016/j.bbrc.2022.10.096.
40. Park, M.; Oh, H.J.; Han, J.; Hong, S.H.; Park, W.; Song, H. Liposome-mediated small RNA delivery to convert the macrophage polarity: A novel therapeutic approach to treat inflammatory uterine disease. *Mol Ther Nucleic Acids* **2022**, *30*, 663-676, doi:10.1016/j.omtn.2022.11.018.
41. Ding, H.; Li, J.; Li, Y.; Yang, M.; Nie, S.; Zhou, M.; Zhou, Z.; Yang, X.; Liu, Y.; Hou, F.F. MicroRNA-10 negatively regulates inflammation in diabetic kidney via targeting activation of the NLRP3 inflammasome. *Mol Ther* **2021**, *29*, 2308-2320, doi:10.1016/j.ymthe.2021.03.012.
42. Valmiki, S.; Ahuja, V.; Paul, J. MicroRNA exhibit altered expression in the inflamed colonic mucosa of ulcerative colitis patients. *World J Gastroenterol* **2017**, *23*, 5324-5332, doi:10.3748/wjg.v23.i29.5324.
43. Wohnhaas, C.T.; Schmid, R.; Rolser, M.; Kaaru, E.; Langgartner, D.; Rieber, K.; Strobel, B.; Eisele, C.; Wiech, F.; Jakob, I., et al. Fecal MicroRNAs Show Promise as Noninvasive Crohn's Disease Biomarkers. *Crohns Colitis 360* **2020**, *2*, otaa003, doi:10.1093/crocol/otaa003.
44. Altaf-Ul-Amin, M.; Karim, M.B.; Hu, P.; Ono, N.; Kanaya, S. Discovery of inflammatory bowel disease-associated miRNAs using a novel bipartite clustering approach. *BMC Med Genomics* **2020**, *13*, 10, doi:10.1186/s12920-020-0660-y.
45. Cho, Y.K.; Son, Y.; Kim, S.N.; Song, H.D.; Kim, M.; Park, J.H.; Jung, Y.S.; Ahn, S.Y.; Saha, A.; Granneman, J.G., et al. MicroRNA-10a-5p regulates macrophage polarization and promotes therapeutic adipose tissue remodeling. *Mol Metab* **2019**, *29*, 86-98, doi:10.1016/j.molmet.2019.08.015.
46. Li, B.; Yang, C.; Zhu, Z.; Chen, H.; Qi, B. Hypoxic glioma-derived extracellular vesicles harboring MicroRNA-10b-5p enhance M2 polarization of macrophages to promote the development of glioma. *CNS Neurosci Ther* **2022**, *28*, 1733-1747, doi:10.1111/cns.13905.

47. Nauck, M.A.; Quast, D.R.; Wefers, J.; Meier, J.J. GLP-1 receptor agonists in the treatment of type 2 diabetes - state-of-the-art. *Mol Metab* **2021**, *46*, 101102, doi:10.1016/j.molmet.2020.101102.
48. Tamborlane, W.V.; Barrientos-Perez, M.; Fainberg, U.; Frimer-Larsen, H.; Hafez, M.; Hale, P.M.; Jalaludin, M.Y.; Kovarenko, M.; Libman, I.; Lynch, J.L., et al. Liraglutide in Children and Adolescents with Type 2 Diabetes. *N Engl J Med* **2019**, *381*, 637-646, doi:10.1056/NEJMoa1903822.